Multiple targeted self-emulsifying compound RGO reveals obvious anti-tumor potential in hepatocellular carcinoma

Sanxiu He,[1,2] Shaorong Tian,[2] Xiaoqian He,[2] Xin Le,[2] Yijiao Ning,[2] Jialin Chen,[3] Hongyi Chen,[4] Junhao Mu,[2] Ke Xu,[2] Qin Xiang,[2] Yue Wu,[2] Jiong Chen,[5] and Tingxiu Xiang[2]

[1]Department of Oncology, The First Affiliated Hospital of Chongqing Medical University, Chongqing, China; [2]Key Laboratory of Molecular Oncology and Epigenetics, The First Affiliated Hospital of Chongqing Medical University, Chongqing, China; [3]Chongqing Traditional Chinese Medicine Hospital, Chongqing, China; [4]Chongqing College of Humanities, Science & Technology, Chongqing, China; [5]College of Pharmacy, Chongqing Medical University, Chongqing, China

Hepatocellular carcinoma (HCC) is a highly vascularized, inflammatory, and abnormally proliferating tumor. Monotherapy is often unable to effectively and comprehensively inhibit the progress of HCC. In present study, we selected ginsenoside Rg3, ganoderma lucidum polysaccharide (GLP), and oridonin as the combined therapy. These three plant monomers play important roles in anti-angiogenesis, immunological activation, and apoptosis promotion, respectively. However, the low solubility and poor bioavailability seriously hinder their clinical application. To resolve these problems, we constructed a new drug, Rg3, GLP, and oridonin self-microemulsifying drug delivery system (RGO-SMEDDS). We found that this drug effectively inhibits the progression of HCC by simultaneously targeting multiple signaling pathways. RGO-SMEDDS restored immune function by suppressing the production of immunosuppressive cytokine and M2-polarized macrophages, reduced angiogenesis by downregulation of vascular endothelial growth factor and its receptor, and retarded proliferation by inhibiting the epidermal growth factor receptor EGFR/AKT/epidermal growth factor receptor/protein kinase B/glycogen synthase kinase-3 (GSK3) signaling pathway. In addition, RGO-SMEDDS showed considerable safety in acute toxicity tests. Results from this study show that RGO-SMEDDS is a promising therapy for the treatment of HCC.

INTRODUCTION

Currently, the treatment for advanced hepatocellular carcinoma (HCC) is extremely limited. Hence, new strategies for liver cancer are urgently needed.[1–3] Because the occurrence of liver cancer involves multiple gene changes and cell abnormalities, monotherapy is often unable to effectively inhibit tumor growth.[4,5] In contrast, multidrug therapy can be more advantageous due to synergies.[6–9]

HCC is a highly vascularized, inflammatory, and abnormally proliferating tumor. Given the inflammatory background of HCC, the hepatic tumor microenvironment (TME) plays a critical role in tumor progression. Therefore, the therapies focusing on the modulation of TME are particularly promising. Ganoderma lucidum polysaccharides (GLPs) are the main bioactive component of a water-soluble extract of the mushroom ganoderma lucidum.[10] GLP has been reported to improve the immune TME by activating immune function.[11–13] HCC also is a hypervascular tumor in which angiogenesis plays an important role in tumor growth and spread. Hence, anti-angiogenic treatment remains the main method in systemic therapy of HCC.[14,15] 20(S)-ginsenoside-Rg3, a natural triterpenoid saponin extracted from red ginseng, has been shown to possess significant anticancer activity by the inhibition of migration and angiogenesis.[16,17] In addition to immune avoidance and angiogenesis promotion, HCC also stimulates proliferation-related signaling pathways and inhibits apoptosis-related signaling pathways to guarantee rapid tumor proliferation. Oridonin, a diterpenoid isolated from the medicinal herb Rabdosia rubescens, has been proven, carrying remarkable anti-proliferation effects.[18–24] Although oridonin appears to be effective for cancer treatment, its underlying mechanism is still very complicated, and direct target requires a fuller disclosure.

In order to improve the therapeutic effect on liver cancer, we used these three before-mentioned plant monomers for combined therapy. However, low bioavailability and poor solubility limit the clinical application of these drugs.[18,19] To resolve these problems, we constructed a new drug, RGO-SMEDDS, which is a self-emulsifying compound comprising RGO (Figure S1). SMEDDS is an isotropic transparent or semi-transparent dispersion system composed of oil phase, emulsifier, and co-emulsifier, which is characterized by the automatic formation of oil-in-water (O/W)-type microemulsion under physiological conditions such as body temperature and gastrointestinal peristalsis. SMEDDS has been shown to improve the solubility and bioavailability of insoluble or fat-soluble drugs, increase absorption rates and

stability, and overcome first-pass effects through lymphatic circulation.[25,26] In this study, the anti-tumor effect and mechanism of RGO-SMEDDS were evaluated in order to provide a new perspective for the treatment of liver cancer.

RESULTS

RGO-SMEDDS inhibits HCC cell proliferation

Functional assays were performed to assess the anti-tumor effects of RGO-SMEDDS. First, we examined the effects of 0, 0.15, 0.30, 0.60, and 1.20 μM RGO-SMEDDS on the proliferation of HCC and LO2 cells by Cell Counting Kit-8 (CCK-8) assay (Figure 1A). RGO-SMEDDS inhibited the proliferation of liver cancer cells in a dose-dependent manner while doing no harm to normal cells within the prescribed concentration range. In order to determine an appropriate administration concentration, we assessed the semi-lethal dose of RGO-SMEDDS for Huh7 and HepG2 cells by 50% inhibitive concentration (IC_{50}) assay (Figure 1B). The RGO-SMEDDS IC_{50}s for Huh7 and HepG2 were 1.2 μM and 2.0 μM, respectively. These doses were also applied for subsequent experiments *in vitro* . Clone-formation assay was used to assess the effects of RGO-SMEDDS on cell viability. RGO-SMEDDS significantly inhibited the viability of Huh7 and HepG2 cells (Figure 1C; Huh7: 84.7%, HepG2: 86.3%; p < 0.001). Detected by flow cytometry (FCM), RGO-SMEDDS dose dependently increased the percentage of cells in the G2/M phase compared to control (Figure 1D). Furthermore, RGO-SMEDDS induced a higher apoptosis rate as judged by FCM with V-fluorescein isothiocyanate (V-FITC) and propidium iodide (PI) staining (Figure 1E). Overall, RGO-SMEDDS effectively produced anti-tumor effects by inhibiting cell proliferation, reducing cell viability, inducing cell cycle arrest, and promoting cell apoptosis.

RGO-SMEDDS suppresses xenograft tumor growth *in vivo*

The above experiments demonstrated the anti-tumor effects of RGO-SMEDDS *in vitro*. To assess the effects of RGO-SMEDDS on HCC *in vivo*, subcutaneous xenograft models were constructed in nude mice and C57B/L mice. As shown (Figures 2A−2F), tumor size of RGO-SMEDDS-treated mice was significantly reduced compared to control mice (Figures 2A, 94.7%, and 2D, 90.0%; p < 0.001), indicating a significant inhibition of liver cancer growth. Furthermore, more obvious nuclear fragmentation and proliferation inhibition was found in the RGO-treated group via hematoxylin and eosin (H&E) staining and the detection of Ki67 by immunochemistry (Figure 2G).

RGO-SMEDDS inhibits HCC migration, invasion, and angiogenesis

The effects of RGO-SMEDDS on metastasis were assessed. By migration assay, RGO-SMEDDS reduced cell migration (Figure 3A; Huh7: 98.5%, HepG2: 94.5%; p < 0.001), and by invasion assay, RGO-SMEDDS significantly weakened the ability of HCC cells to invade barriers (Figure 3B; Huh7: 96.6%, HepG2: 84.5%; p < 0.001). The effect of RGO-SMEDDS on angiogenesis was measured by tubule formation assay (Figure 3C). Human Umbilical Vein Endothelial Cells (HUVECs) were cultured in conditioned medium of HepG2 and Huh7 cells treated with or without RGO-SMEDDS for 48 h. RGO-SMEDDS significantly inhibited angiogenesis induced by HepG2 and Huh7 cells. In addition, we performed quantitative reverse transcriptase-PCR (qRT-PCR) and western blot (WB) analysis to investigate the mechanism of RGO on angiogenesis (Figures 3D and 3E). Compared to control, the expression of vascular endothelial growth factor (VEGF) and VEGF receptor (VEGFR) in RGO-SMEDDS-treated HCC cells and tissues was significantly downregulated. Similar results were found by immunohistochemistry (IHC), where RGO-SMEDDS significantly downregulated VEGF and VEGFR levels in tumor tissues (Figure 3F). Further, the number of blood vessels in the treated group was much less than that in control. Taken together, these results demonstrated RGO-SMEDDS can effectively inhibit the migration, invasion, and angiogenesis tendency of HCC cells.

RGO-SMEDDS inhibits immunosuppressive cytokines and M2 macrophages

The qRT-PCR and WB assays were used to assess cytokine expression levels in HCC cells treated with or without RGO-SMEDDS (Figures 4A and 4B). As results suggest, RGO-SMEDDS significantly reduced the expression levels of interleukin (IL)-2, IL-4, IL-10, IL-13, and macrophage colony stimulating factor 1 (M-CSF1), which are closely related to M2 macrophage differentiation. Based on these results, we speculated that RGO-SMEDDS inhibited M2-polarized macrophage induced by HCC cells. In order to verify this speculation, we added RGO-SMEDDS to the THP1-HCC co-culture system and examined the mRNA expression level of M2 macrophage markers in THP1 cells by qRT-PCR (Figure 4C). The expression levels of IL-10, CD163, and arginase 1 (Arg1) were significantly downregulated in THP1 cells from the RGO-SMEDDS-added co-culture system. Moreover, we found RGO-SMEDDS directly inhibited IL-10, CD163, and Arg1 in THP1 cells, indicating that RGO-SMEDDS could not only prevent the M2-polarized macrophage induced by HCC cells but also directly inhibit the formation of M2 macrophages. IHC was used to assess the proportion of M2-like macrophages surrounding tumor tissues (Figure 4D), and the results demonstrated the number of M2 macrophages to be significantly less in RGO-SMEDDS-treated mice compared to control. Therefore, it can be concluded that RGO-SMEDDS improved the immunosuppressive microenvironment by inhibiting the M2-polarized macrophages.

Epidermal growth factor receptor (EGFR) may be a potential target of oridonin

In order to explore the anti-tumor mechanism of oridonin, the 3D structure (obtained from PubChem) was introduced to predict oridonin targets by PharmMapper (Figure 5A). Predictive oridonin targets analyzed by Gene Ontology (GO) enrichment were mainly tyrosine kinases, which are closely related to tumor occurrence and development (Figures 5B and 5C). AutoDock 1.1.2 software was used to simulate molecular docking between oridonin and the tyrosine kinase receptor, EGFR (Figures 5D−5F). We found oridonin can form hydrogen bonds with the amino acid residue, Arg841, and form hydrophobic interactions with amino acid residues Cys797, Val726,
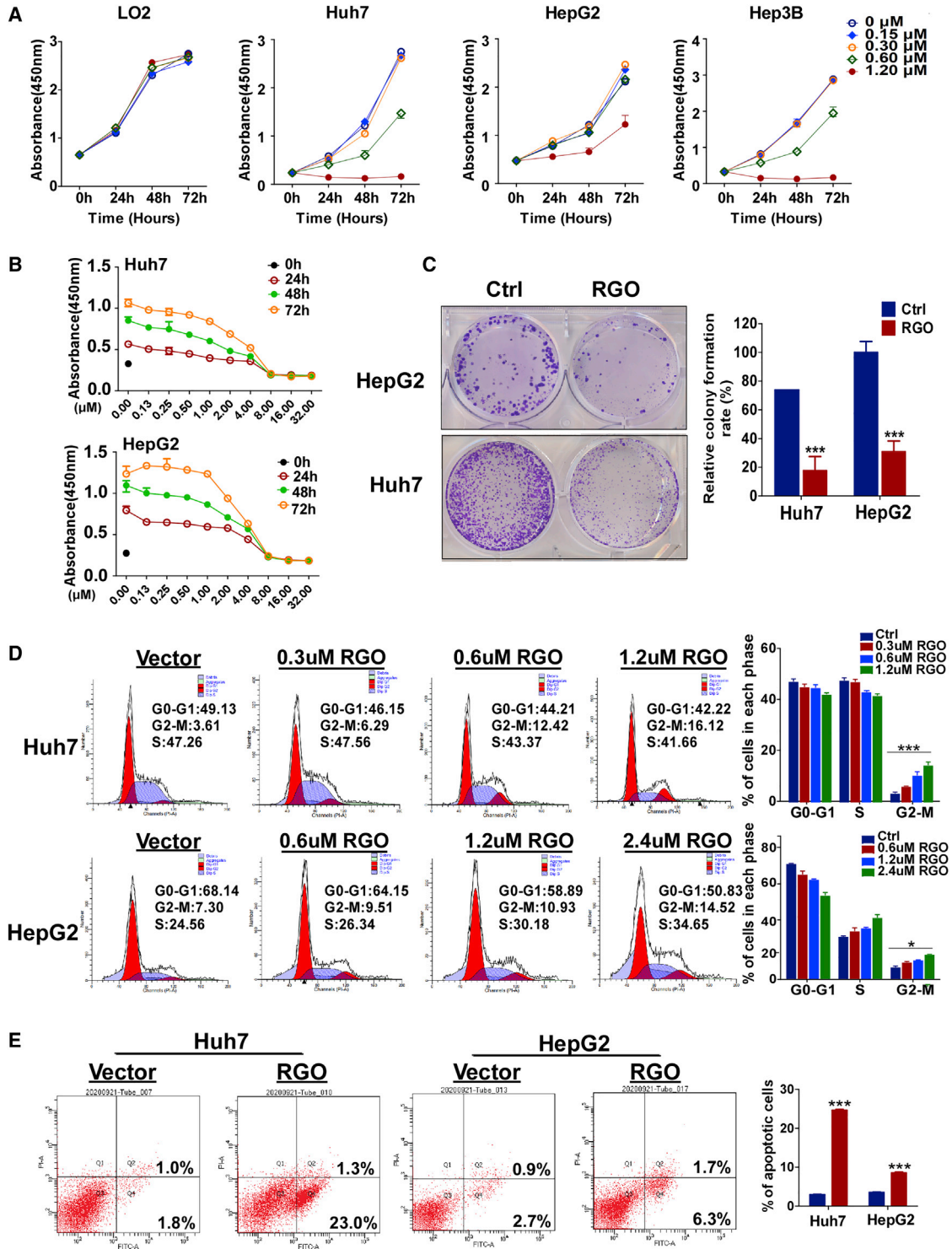
Figure 1. Role of RGO-SMEDDS on hepatoma carcinoma cell growth *in vitro*

(A) Measurement of cell proliferation for 0, 0.15, 0.30, 0.60, and 1.20 μM RGO-SMEDDS-treated LO2, Huh7, HepG2, and Hep3B cells by CCK-8 assay. (B) IC_{50} of RGO-SMEDDS against HepG2 and Huh7 cells. (C) Effects of RGO-SMEDDS on the colony formation of HepG2 and Huh7 cells. (D) Cell cycle distribution of RGO-SMEDDS treated at different concentrations of Huh7 and HepG2 cells determined by flow cytometry. (E) Flow cytometry was used to detect apoptosis induced by RGO-SMEDDS. Values are shown as mean ± standard error from three independent experiments. *$p < 0.05$, **$p < 0.01$, ***$p < 0.001$.
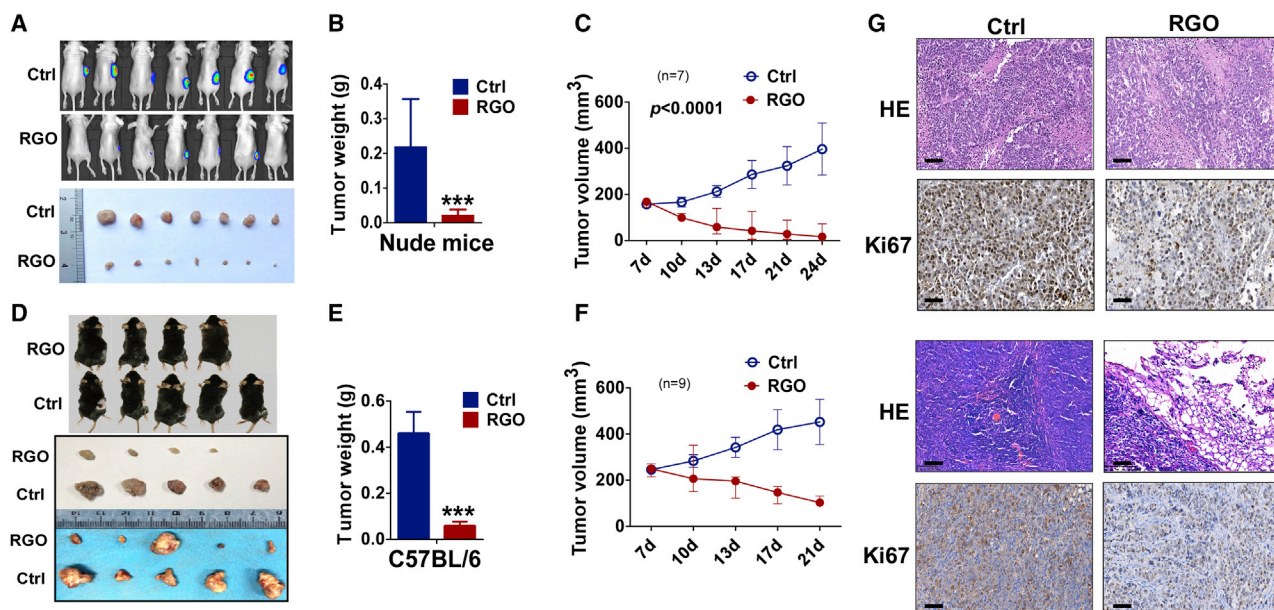
Figure 2. RGO-SMEDDS suppresses xenograft liver tumor growth *in vivo*

(A) Representative images of xenograft tumor status assessed by *in vivo* fluorescence imaging (upper) or viewing with naked eye (lower). (B and C) Tumor weight by the time of resection and tumor volume growth curve in nude mice. Tumor volume was calculated from tumor length and width, measured every 2 days. (D) Representative pictures of the xenograft tumors before and after resection in comparison between RGO and the control group. (E and F) Growth curve and weight of xenograft tumors in C57BL/6 mice. Tumor volume was calculated from tumor length and width, measured every 2 days. (G) H&E staining and immunohistochemistry (IHC) staining of Ki67 of xenograft tumor tissues from nude mice and C57BL/6 mice. Scale bars, 60 μm. The data are shown as the mean ± SD. *p < 0.05, **p < 0.01, ***p < 0.001.

and Leu844. Moreover, oridonin fits well within the activation cavity of EGFR (docking score −7.2 kcal/mol). These results suggest oridonin may be a potential inhibitor of EGFR.

RGO-SMEDDS suppresses proliferation via the EGFR/AKT/ glycogen synthase kinase-3 (GSK3) signaling pathways

According to the results of bioinformatics analysis, we speculated that RGO-SMEDDS could act on EGFR. To prove this conjecture, we performed immunohistochemical staining on mouse tumor tissues. The results showed that the expression levels of EGFR and EGFR phosphorylation (p)-EGFR in the RGO-SMEDDS group were significantly lower than those in the control group (Figure 6A). In addition, WB results showed that RGO-SMEDDS treatment could partially inhibit EGF-induced activation of EGFR. We also detected the expression of downstream molecules in the EGFR pathway, and the results showed that RGO-SMEDDS could effectively inhibit the AKT/GSK3 signaling pathway, and EGF treatment partially reversed this phenomenon (Figure 6B). The AKT/GSK3 signaling pathway is closely related to cell proliferation, so we tested whether RGO-SMEDDS plays an anti-proliferation role by inhibiting this signaling pathway. The results of qRT-PCR and WB showed that RGO-SMEDDS effectively inhibited the expression level of HCC stem cell markers, and AKT activator SC79 reversed this effect (Figures 6C and 6D). In addition, the sphere-formation assay and clone-formation assay showed that RGO-SMEDDS treatment effectively inhibited the proliferation activity of HCC cells, and this effect could be partially reversed by SC79 (Figures 6E and 6F). These results demonstrated RGO-

SMEDDS can inhibit the proliferation of HCC cells by inhibiting the EGFR/AKT/GSK3 signaling pathway.

RGO-SMEDDS is a safe and effective anti-tumor drug

Within 14 days after administration, the mice in the 1,000 mg/kg group showed sluggish activity within 2−3 h after administration, and the other group (0, 100, 200 mg/kg) was in good condition without significant weight loss. To assess RGO-SMEDDS toxicity, H&E staining was performed on tissue sections of major organs. No histopathological changes were found in the brain, gastric, colon, heart, liver, spleen, lung, or kidney tissues, indicating that RGO-SMEDDS has a relatively low degree of toxicity (Figure S2). Since no half-lethal dose (LD50) of RGO-SMEDDS was found, we performed an LD50 test with the maximum dose (1,000 mg/kg). The results of H&E staining were shown in Figure 7 and are consistent with previous experiments.

DISCUSSION

HCC is one of the most aggressive cancers with an extremely low survival rate and a high risk for metastasis. Diagnosis is frequently conducted during late stages of this disease when treatment is extremely poor.[27] The molecular mechanisms involved in tumorigenesis are multi-faceted and complex, which tend to result in tolerance to monotherapy.[28] Hence, combinatorial therapies are employed to maximize treatment efficacy.[6] Herein, RGO-SMEDDS was shown to have superior therapeutic efficacy against HCC both *in vitro* and *in vivo*. RGO-SMEDDS acts by targeting multiple anti-tumor
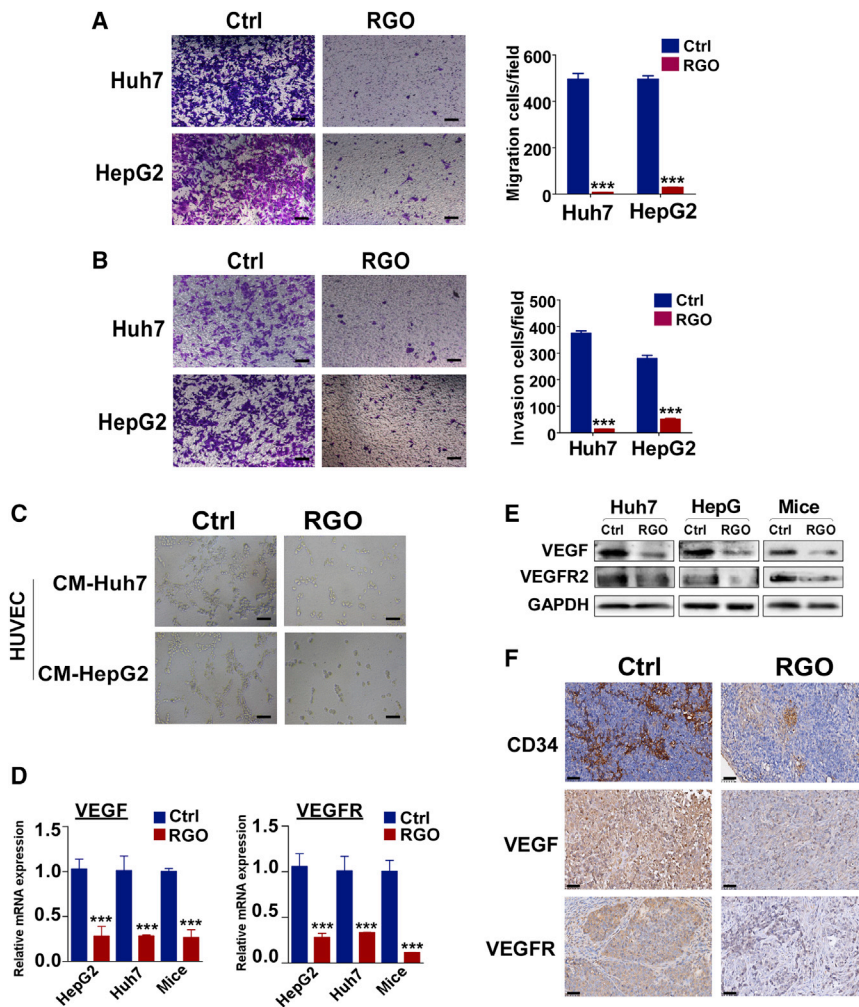
anti-tumor effects suggest a role for RGO-SMEDDS as a novel and effective candidate for liver cancer treatment.

Tumor cells typically induce an immune-tolerant TME by secretion of suppressive molecules such as IL-10, transforming growth factor (TGF)-β, prostaglandin E2, and VEGF.[42] In addition, tumor cells have been reported to induce M2-like differentiation of macrophages to reduce immune attack by secretion of the cytokines IL-4, IL-10, and M-CSF.[43–45] Macrophages, called Kupffer cells in the liver, inhibit the early development of HCC; however, during tumor progression, M1 switch to M2, leading to adaptive immune system suppression and tumor support.[46,47] Furthermore, M2 macrophages promote tumor progression and metastasis, and tumor-associated macrophage (TAM) infiltration is associated with poor prognosis in liver cancers.[48] In this study, RGO-SMEDDS treatment inhibited HCC secretion of the immunosuppressive cytokines IL-4, IL-10, IL-13, and M-CSF. This inhibition effectively blocked the induction of M2-like macrophage differentiation by HCC cells, resulting in improved anti-tumor immune function.

EGFR, a member of receptor tyrosine kinase (RTK) family, has emerged as an important therapeutic target.[49] Overexpression of EGFR is frequently observed in HCC, suggesting that EGFR might play an important role in HCC pathogenesis and treatment.[50] In this study, we predicted, by use of the PharmMapper website and molecular docking assay, that EGFR may be the potential target of oridonin. WB assay showed that RGO-SMEDDS inhibited p-EGFR and its downstream signaling molecule AKT. Previous studies have shown that tumor cells expressing low levels of EGFR and laryngeal squamous cell carcinoma cells with EGFR knockdown are less sensitive to oridonin.[51] In addition, oridonin has been shown to inhibit

mechanisms: (1) altering the immune-tolerant TME by reducing the production of immune-suppressive cytokines and M2-polarized macrophages; (2) exerting an anti-angiogenic effect by downregulating VEGF and VEGFR expression; (3) exerting anti-proliferative effects by inhibiting the EGFR/AKT signaling pathway. Based on various studies, anti-angiogenic drugs combined with immunotherapy are a promising cancer treatment strategy.[29,30,31] Anti-angiogenic drugs may recover the host's potent anti-tumor immune response by interfering with multiple steps of the cancer immunity cycle. These include promotion of antigen presentation and lymphocyte infiltration,[32–35] activation of cytotoxic CD8+ T cells, and immune-suppression reduction.[36–38] On the other hand, immunotherapy reduces tumor vascular density, improves vessel perfusion, alleviates tumor tissue hypoxia, and promotes normalization of the tumor vasculature.[36,37] In addition, immunosuppressive microenvironments weaken the effect of pro-apoptotic drugs through adaptive resistance, and an abnormal blood supply affects the entry of pro-apoptotic drugs into tumor tissue. As such, immune and angiogenesis therapies are also indispensable when growth inhibitors are used for treatment.[39–41] These
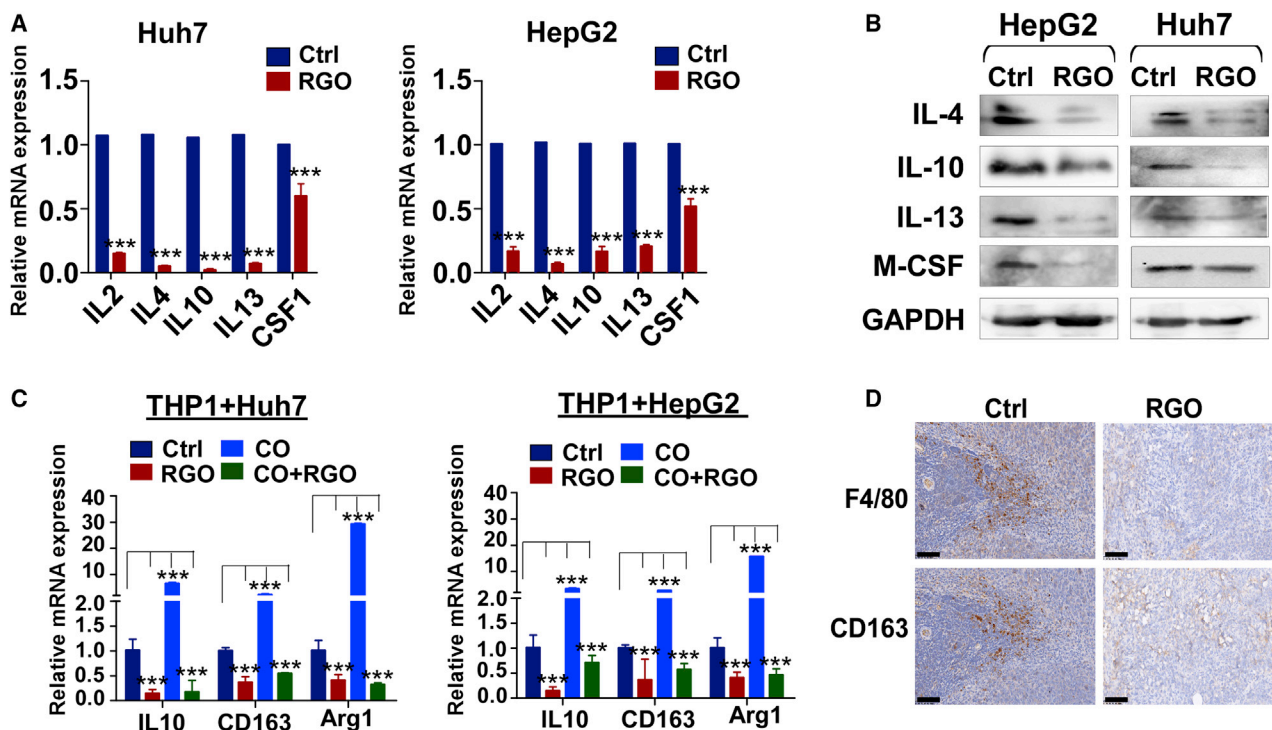
Figure 4. Effects of RGO-SMEDDS on immune microenvironment of HCC

(A and B) qRT-PCR analyses and WB assays were used to detect the expression level of immunosuppressive cytokines in RGO-SMEDDS-treated and untreated HCC cells. (C) The mRNA expression level of M2 markers of THP-1 cells in the co-culture system with or without RGO-SMEDDS. CO, co-culture. (D) IHC staining of F4/80 and CD163 was used to detect the infiltration of M2 macrophages in tumor tissues of the control group and the RGO-SMEDDS-treated group. Scale bars, 70 μm. Values are shown as mean ± standard error from three independent experiments. *p < 0.05, **p < 0.01, ***p < 0.001.

EGFR-mediated phosphatidylinositol 3-kinase (PI3K)/AKT and Ras/Raf/MEK/ERK pathways,[52,53] which is consistent with our results. GSK3, major targets correlated with the PI3K/AKT pathway, is involved in the regulation of tumor cell proliferation. Therefore, we analyzed the effect of RGO-SMEDDS on the proliferation of HCC. Results showed that RGO-SMEDDS inhibited cell proliferation and downregulated the expression levels of stemness markers. Cancer stem cells (CSCs) have been shown as the main cause of treatment resistance and cancer recurrence due to pluripotency and self-renewal ability.[54] Further, CSCs have been implicated in cancer cell growth, invasion/metastasis, vasculogenesis, and immunosuppression.[55] Hence, RGO-SMEDDS inhibition of tumor cell stemness may benefit patients with liver cancer.

Combinatorial treatment of cancer has provoked widespread concern because of the associated challenges such as plasma instability, low bioavailability, and systemic toxicity. In this study, in addition to its excellent anti-tumor effects, RGO-SMEDDS has been shown to be safe in acute toxicity tests. When the mice were given a large dose of 1,000 mg/kg, no pathological changes occurred in important organs. This dose was 100 times that of the actual clinical dosage, indicating that RGO-SMEDDS has no obvious toxic side effects. The safety of RGO-SMEDDS may be attributed to the following: (1) RGO is less toxic as a natural drug;[56,61] (2) synergistic effects among

drugs reduce the unnecessary drug amount while still achieving equal efficiency;[4,6] (3) SMEDDS improve the bioavailability of drugs.[18,62,63]

In summary, we investigated the functional role and molecular mechanism of RGO-SMEDDS as a potential treatment for HCC. The results showed RGO-SMEDDS effectively played an anti-tumor role both *in vivo* and *in vitro*, with good safety. RGO-SMEDDS promoted apoptosis, inhibited angiogenesis, reduced the release of immunosuppressive cytokines, and decreased the proportion of M2-polarized macrophages. In addition, RGO-SMEDDS inhibited the p-EGFR and the activation of downstream AKT/GSK3 signaling pathways. These results suggested that RGO-SMEDDS may be a potentially effective treatment strategy for improving the survival of HCC patients.

MATERIALS AND METHODS

Chemicals

Ginsenoside RGO used in this study was obtained from Nanjing Zelang Medical Technology (Nanjing, China). Soybean lecithin was a product of Tianjin Kwangfu Fine Chemical Industry Research Institute (Tianjin, China). Ethyl oleate was purchased from Shandong Jining Hongming Chemical Reagent (Shandong, China), and span-80 was purchased from Chengdu Kelong Chemical Reagent Factory (Chengdu, China).
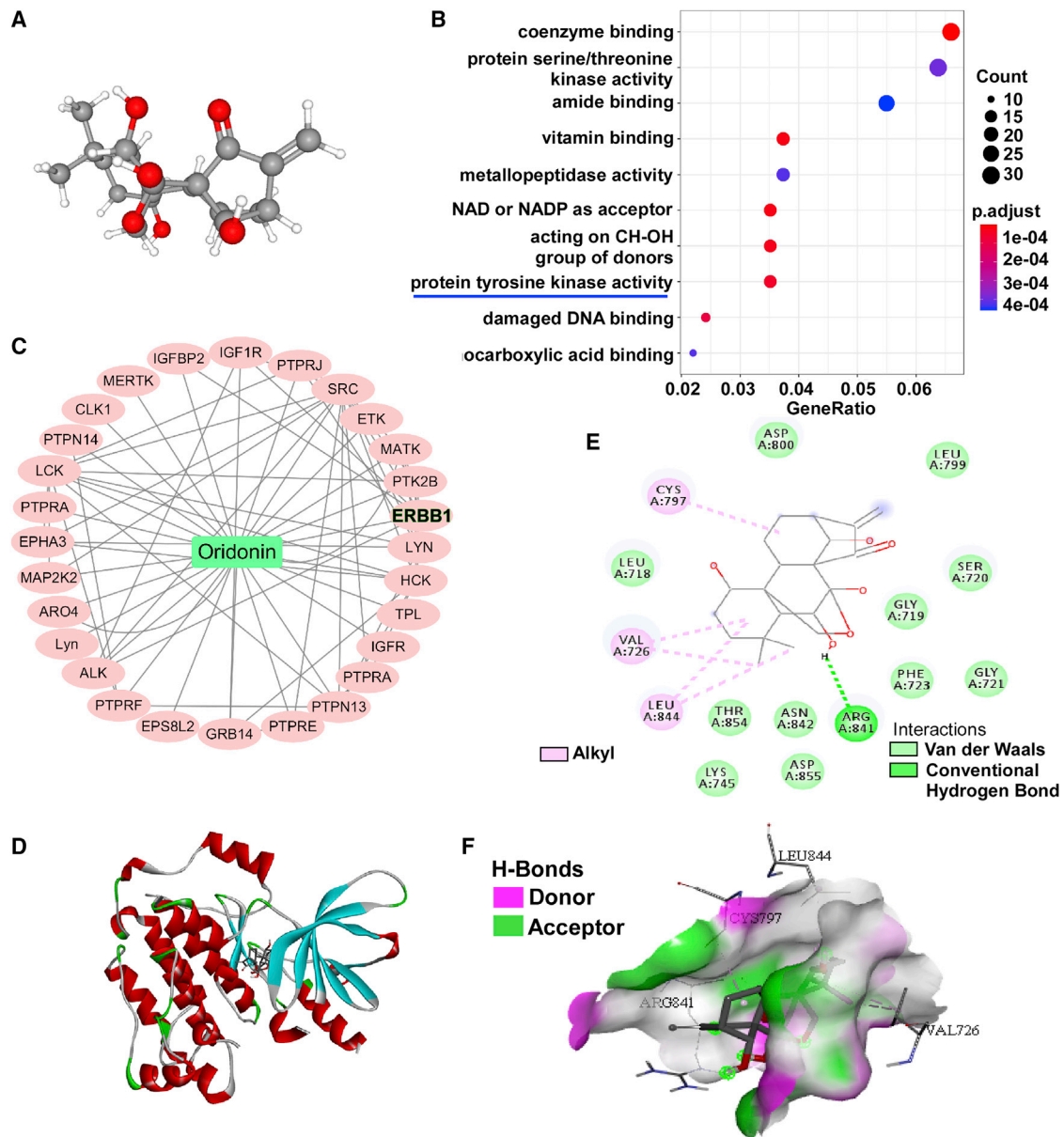
Figure 5. Target prediction of oridonin

(A) The 3D structure of oridonin was obtained from the PubChem database. (B) GO pathway enrichment analysis of the predicted targets of oridonin was demonstrated by dotplots. (C) The PPI network of tyrosine kinase-related protein networks among the predicted targets of oridonin. (D) Docking poses into the pharmacophore of EGFR tyrosine kinase domain (PDB: -5GNK, in red cartoon representation). Oridonin was represented in gray. (E) The 2-dimensional schematic diagram of interactions of EGFR with oridonin. (F) The pocket view of EGFR binding with oridonin.

Preparation of RGO-SMEDDS

6 mg/mL ginsenoside Rg3, 20 mg/mL GLP, and 20 mg/mL oridonin were added into the mixture of tetrahydrofuran and 50 mg/mL soybean lecithin and stirred at 55°C∼65°C at a constant speed until completely dissolved. The lecithin complex was formed after the removal of tetrahydrofuran by rotary evaporation. With ethyl oleate as the oil phase, Tween 80 as the emulsifier, and polyethylene glycol-400 as the solvent, a ternary phase diagram was used to construct the self-emulsifying sys-tem of RGO. The lecithin complex was added to the mixed system of oil phase, emulsifier, and solvent in a ratio of 2:5:2. The mixture was then stirred at 37°C∼45°C and 100∼500 rpm/min until a light blue trans-parent liquid was formed (patent number [no.]: ZL 2020 1 0439015.3).

Cell lines

Cell lines (HepG2, Huh7, Hep3B, LO2, and THP-1) were obtained from the American Type Culture Collection (ATCC; Manassas,
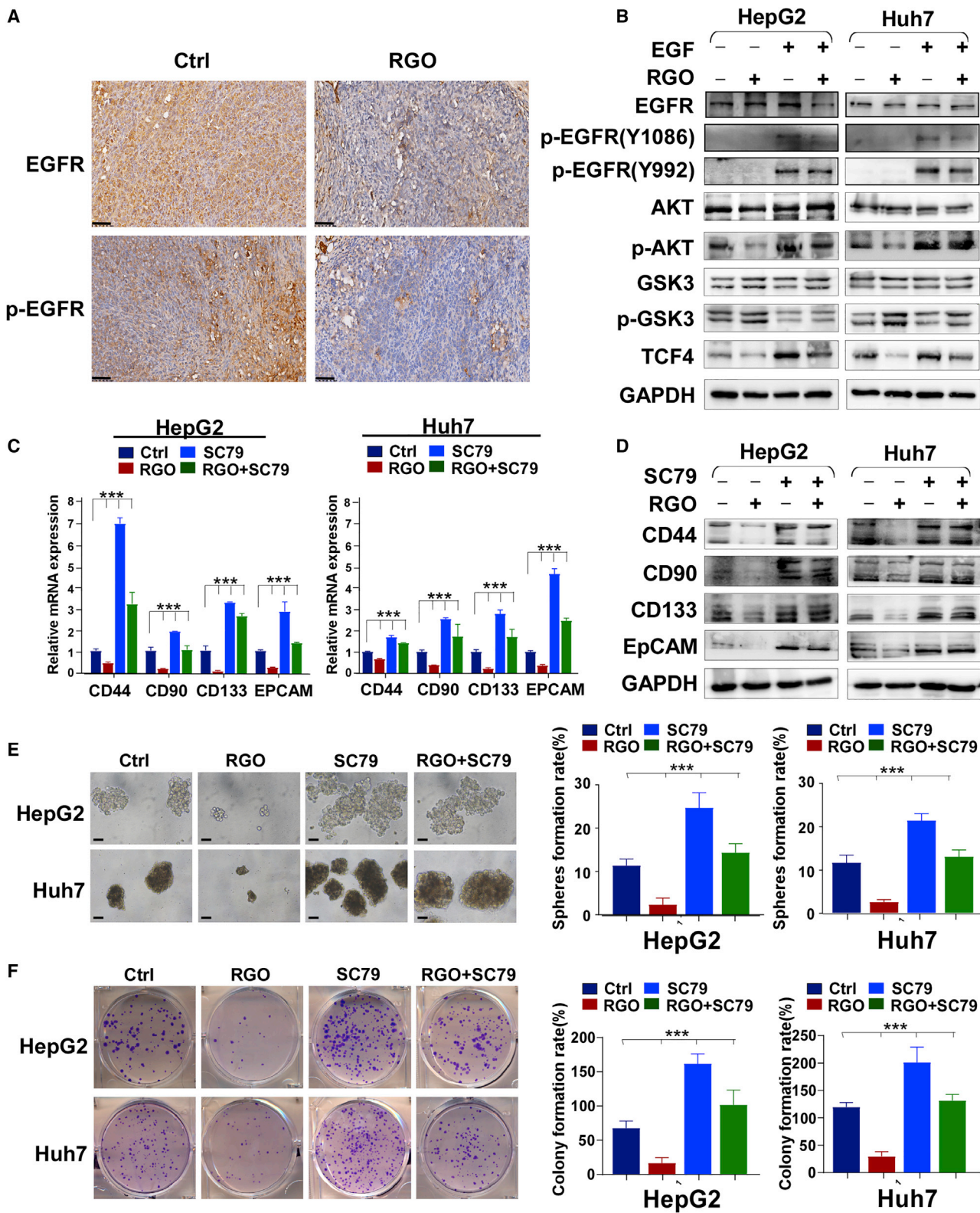
(legend on next page)

VA, USA) or collaborators. Cells were cultured in RPMI-1640 medium (Gibco-BRL, Karlsruhe, Germany) supplemented with 10% fetal bovine serum (FBS) plus 1% penicillin and streptomycin at 37°C/5% CO_2, as advised by ATCC.

RNA isolation, RT-PCR, and real-time PCR
Total RNA isolation was achieved by using TRIzol Reagent (Molecular Research Center, Cincinnati, OH, USA) and the manufacturer's instructions. RT-PCR was performed to generate cDNA in a total volume of 20 μL. RT-PCR was performed using Go-Taq (Promega, Madison, WI, USA) with the following conditions: initial denaturation at 95°C for 2 min and 32 amplification cycles (denaturation: 95°C for 30 s; annealing: 55°C for 30 s; and extension: 72°C for 30 s), with final extension at 72°C for 3 min. β-actin was used as an internal control with only 23 cycles for amplification. RT-PCR was accomplished with a SYBR Green kit (Thermo Fisher Scientific) and a 7500 Real-Time PCR System (Applied Biosystems, Foster City, CA, USA). Specific primer sequences are listed in Table 1, with p values for each group determined by Student's t test. Each sample was assessed in three independent experiments.

Cell proliferation and colony formation assays
HepG2 and Huh7 cells were seeded into 96-well plates at a density of 2,000/well. The effect of RGO-SMEDDS was assessed at concentrations of 0, 0.15, 0.30, 0.60, and 1.20 μM. Cell proliferation at different time periods (0, 24, 48, and 72 h) was measured by absorbance at 450 nm with a CCK-8 (Beyotime, Shanghai, China). For the colony formation assay, HepG2 and Huh7 were placed into 6-well plates with increasing concentrations of RGO-SMEDDS (200, 400, and 800/well). After 14 days of incubation, cell colonies were stained with crystal violet and evaluated by scanning with a CanoScan 8800F MOEL-85 scanner.

FCM
Cell cycle and apoptotic status was estimated by FCM. For apoptosis, cells were treated with or without RGO-SMEDDS, harvested, and double stained with PI and annexin V-FITC. For cell cycle analysis, cells were collected and fixed with ice-cold 75% ethanol, treated with RNase, and stained with PI. Three individual samples were assessed for each group.

Nude mouse tumor xenograft model
This research was approved by the Institutional Ethics Committees of the First Affiliated Hospital of Chongqing Medical University (Approval notice: # 2018-77) and conformed to the tenets of the Declaration of Helsinki. 1×10^7 HepG2 cells were subcutaneously injected into nude mice (male, n = 14) and 1×10^6 Hep1-6 cells into

C57BL/6 mice (male, n = 20). Mice were randomly divided into control and treated groups on the 5th day after transplantation. The treated group was given 10 mg/kg RGO-SMEDDS orally every day for 2 weeks, whereas the control group was treated with an equal volume of PBS. Tumor size was measured every 2 days. During the next 30 days, a vernier caliper was used to measure tumor size (as judged by length and width) every 3 days. Tumor volume was determined using the formula: volume = length $\times$ width^2 $\times$ 0.52.

Transwell and wound healing assays for cell migration and invasion
Cell migration was assessed by Transwell and wound healing assays as previously described.[64] Transwell chambers were purchased from Corning (Corning, Kennebunk, ME, USA). For the invasion assay, Matrigel glue (BD Biosciences) was placed on the upper surface of the chambers. The cells on the chamber's lower surface were assessed by phase-contrast microscopy (Leica), 24 h after seeding. All experiments were conducted in triplicate.

WB
Protein lysates (40 μg) were separated by sodium dodecyl sulfate-polyacrylamide gel electrophoresis (SDS-PAGE) and transferred to polyvinylidene difluoride (PVDF) membranes. The primary antibodies used were reactive with VEGF (#ab1316; Abcam), VEGFR (#ab11939; Abcam), AKT (#ab38449; Abcam), p-AKT (#ab8805; Abcam), GSK3 (#sc-7291; Santa Cruz Biotechnology), p-GSK3 (#sc-81496; Santa Cruz Biotechnology), EGFR (sc373746; Santa Cruz), and p-EGFR (sc-377547; Santa Cruz). Secondary antibodies were used at a dilution of 1:2,000 at room temperature. Protein bands were visualized by the Immobilon Western Chemiluminescent HRP Substrate Kit (Millipore, Billerica, MA, USA).

IHC staining
Tissues were fixed in 4% paraformaldehyde, sent for sectioning, and assessed with an IHC kit (ZSGB-BIO, Beijing, China). Slides were incubated at 4°C overnight (16−20 h) with antibodies reactive with Ki67 (#ab16667; Abcam), F4/80 (#ab100790; Abcam), CD163 (#sc58965; Santa Cruz), VEGF (#ab32152; Abcam), VEGFR (#ab32152; Abcam), CD34 (#ab81289; Abcam), EGFR (#sc373746; Santa Cruz), and p-EGFR (#sc-377547; Santa Cruz). Diaminobenzidine (K176810E; ZSGB-BIO, China) was used for target protein staining and H&E for nuclear staining. Images were photographed at 400× with a microscope.

Tube formation assay
A tube formation assay was used to assess angiogenesis. Matrigel assay kits (Chemicon, Millipore) were used per the manufacturer's

---

Figure 6. RGO-SMEDDS restrains stemness of HCC through the EGFR/AKT signaling pathway
(A) Representative IHC staining results of EGFR and p-EGFR in xenografts. Scale bars, 50 μm. (B) The effect of RGO-SMEDDS on EGFR signaling pathway in HepG2 and Huh7 cells was detected by WB assay. (C and D) The mRNA and protein expression level of stemness markers in RGO-SMEDDS-treated or untreated HepG2 and Huh7 cells determined by WB and qRT-PCR assay under the influence of Akt activator SC79. (E and F) Effects of RGO-SMEDDS and Akt activator SC79 alone or in combination on sphere-forming and clone-forming ability of cells. Scale bars, 50 μm. Values are shown as mean ± standard error from three independent experiments. *p < 0.05, **p < 0.01, ***p < 0.001.
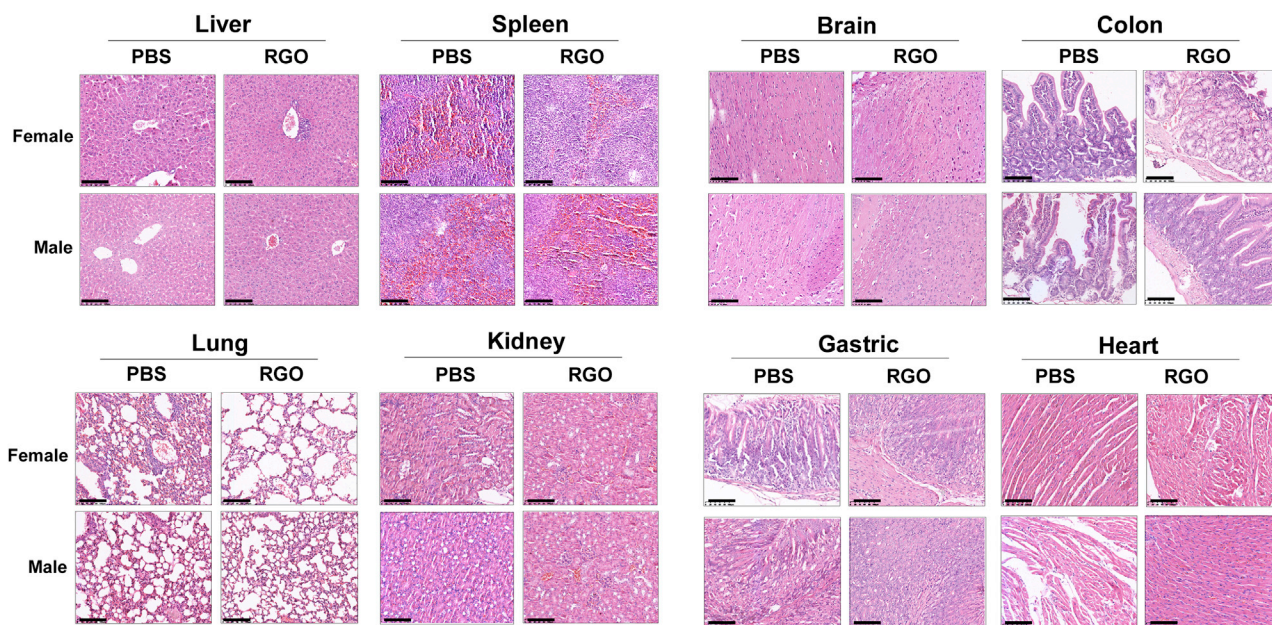
Figure 7. Safety evaluation of RGO-SMEDDS in healthy C57BL/6 mice

Representative images of H&E staining of major organs (liver, spleen, brain, colon, lung, kidney, gastric, and heart) on day 14 after PBS or 1,000 mg/kg RGO treatment. Scale bars, 50 μm.

instructions. Matrigel was allowed to solidify inside an incubator for 30 min. Then, 20,000 HUVECs/well were transferred to chilled pellets and further incubated with conditioned medium derived from HCC cells treated with or without RGO-SMEDDS for 6–24 h. To determine angiogenesis, a branching index for each group was determined at the termination of drug usage.

Sphere-forming assay

Nonadherent dishes (Costar, Corning, NY, USA) were used for this assay. Cells were plated and maintained in serum-free medium (SFM) consisting of DMEM-F12 (Gibco, Carlsbad, CA, USA), 30 ng/mL EGF (Sino Biological; #10605), 15 ng/mL basic fibroblast growth factor (Sino Biological; #10014), 10 μg/mL insulin (Sino Biological; #11038), 0.4% BSA (Sigma-Aldrich, St. Louis, MO, USA), and 2% B27 (Gibco, Carlsbad, CA, USA). Photographs were obtained and the number of spheres assessed by microscopy (Nikon, Tokyo, Japan).

Target prediction of oridonin

The 3D structure of oridonin was obtained from the PubChem database. The PharmMapper server was used for target prediction of oridonin. The R software was used for the GO enrichment analyses of the drug targets. p < 0.01 was set as the threshold, and the 10 top-ranked biological processes were shown. The Protein-Protein Interaction Networks (PPI) analysis of tyrosine kinase-related targets was performed using the string software. Network visualization and analysis are performed using Cytoscape software. The PDB format structure of the EGFR protein (PDB: 5GNK5GNK) is downloaded from the Research Collaboratory for Structural Bioinformatics database. Auto-

Dock Tools 1.5.6 software was used for hydrogenation, charge calculation, atom-type distribution, etc. Finally, AutoDock Vina 1.1.2 was used for molecular docking, and Discovery Studio 2020 was used for visual analysis.

RGO *in vivo* toxicity

This research was approved by the Institutional Ethics Committees of the First Affiliated Hospital of Chongqing Medical University (Approval notice: # 2018-77) and conformed to the tenets of the Declaration of Helsinki. 40 C57BL/6 mice aged 6–8 weeks were randomly divided into four groups (n = 10, one-half male and one-half female) and given a single oral dose of 0, 100, 200, or 1,000 mg/kg of RGO. The LD50 assay was performed with the maximum dose (1,000 mg/kg). Twenty mice were randomly divided into control and treated groups (n = 10). The treated group received oral RGO, 1,000 mg/kg, once. The mental state and activity of the mice were observed daily and their weight measured once a week. All mice were sacrificed 14 days after drug administration. Collectable organs including brain, heart, lungs, stomach, pancreas, liver, kidneys, ovaries, uterus, bowel, and spleen were harvested right after sacrifice. Samples were prepared with formalin and embedded with paraffin using a Ventana machine.

Statistical analyses

All statistical analyses were assessed as mean with SPSS software (version 16; SPSS, Chicago, IL, USA). χ^2 and Fisher's exact tests were utilized for p value calculation. Data were considered statistically meaningful at p < 0.05.

Table 1. List of primers used in this study

PCR	Primer	Sequence (5′—3′)	Product size (bp)	Annealing temperature (°C)
	IL2F	TACAAGAACCCGAAACTGACTCG	223	60
	IL2R	ACATGAAGGTAGTCTCACTGCC		
	IL4F	CCAACTGCTTCCCCCTCTG	150	60
	IL4R	TCTGTTACGGTCAACTCGGTG		
	IL10F	GACTTTAAGGGTTACCTGGGTTG	112	60
	IL10R	TCACATGCGCCTTGATGTCTG		
	IL13F	GAAGGCTCCGCTCTGCAAT	75	60
	IL13R	TCCAGGGCTGCACAGTACA		
	M-CSFF	TGGCGAGCAGGAGTATCAC	108	60
	M-CSFR	AGGTCTCCATCTGACTGTCAAT		
	CD163F	TTTGTCAACTTGAGTCCCTTCAC	127	60
	CD163R	TCCCGCTACACTTGTTTTCAC		
	ARG1F	GTGGAAACTTGCATGGACAAC	76	60
	ARG1R	AATCCTGGCACATCGGGAATC		
qRT- PCR	VEGFAF	AGGGCAGAATCATCACGAAGT	75	60
	VEGFAR	AGGGTCTCGATTGGATGGCA		
	VEGFRF	GGCCCAATAATCAGAGTGGCA	109	60
	VEGFRR	CCAGTGTCATTTCCGATCACTTT		
	SOX2F	GCCGAGTGGAAACTTTTGTCG	155	60
	SOX2R	GGCAGCGTGTACTTATCCTTCT		
	NANOGF	TTTGTGGGCCTGAAGAAAACT	116	60
	NANOGR	AGGGCTGTCCTGAATAAGCAG		
	CD133F	AGTCGGAAACTGGCAGATAGC	99	60
	CD133R	GGTAGTGTTGTACTGGGCCAAT		
	OCT3/4F	CTGGGTTGATCCTCGGACCT	243	60
	OCT3/4R	CCATCGGAGTTGCTCTCCA		
	c-MycF	GGCTCCTGGCAAAAGGTCA	119	60
	c-MycR	CTGCGTAGTTGTGCTGATGT		
	β-actinF	GTCTTCCCCTCCATCGTG	113	60
	β-actinR	AGGGTGAGGATGCCTCTCTT		

AUTHOR CONTRIBUTIONS
T.X. conceived and designed the manuscript. T.X. and S.H. performed the majority of experiments, drafted the manuscript, and reviewed data and the manuscript. T.X., S.H., S.T., J.M., Q.X., and Y.W. performed experiments and analyzed data. Jialin Chen, H.C., and Jiong Chen prepared RGO-SMEDD. T.X., S.H., X.L., K.X., and Y.N. reviewed data and finalized the manuscript. All authors reviewed and approved the final version.

DECLARATION OF INTERESTS
The authors declare no competing interests.

REFERENCES

1. Siegel, R.L., Miller, K.D., and Jemal, A. (2019). Cancer statistics, 2019. CA Cancer J. Clin. *69*, 7–34.

2. Yang, J.D., Hainaut, P., Gores, G.J., Amadou, A., Plymoth, A., and Roberts, L.R. (2019). A global view of hepatocellular carcinoma: trends, risk, prevention and management. Nat. Rev. Gastroenterol. Hepatol. *16*, 589–604.

3. Hidalgo, M., Cascinu, S., Kleeff, J., Labianca, R., Löhr, J.M., Neoptolemos, J., Real, F.X., Van Laethem, J.-L., and Heinemann, V. (2015). Addressing the challenges of pancreatic cancer: future directions for improving outcomes. Pancreatology *15*, 8–18.

4. Parhi, P., Mohanty, C., and Sahoo, S.K. (2012). Nanotechnology-based combinational drug delivery: an emerging approach for cancer therapy. Drug Discov. Today *17*, 1044–1052.

5. Kobayashi, Y., Lim, S.O., and Yamaguchi, H. (2020). Oncogenic signaling pathways associated with immune evasion and resistance to immune checkpoint inhibitors in cancer. Semin. Cancer Biol. *65*, 51–64.

6. Gregory, J.V., Vogus, D.R., Barajas, A., Cadena, M.A., Mitragotri, S., and Lahann, J. (2020). Programmable Delivery of Synergistic Cancer Drug Combinations Using Bicompartmental Nanoparticles. Adv. Healthc. Mater. *9*, e2000564.

7. Yap, T.A., Omlin, A., and de Bono, J.S. (2013). Development of therapeutic combinations targeting major cancer signaling pathways. J. Clin. Oncol. *31*, 1592–1605.

8. André, F., Bachelot, T., Commo, F., Campone, M., Arnedos, M., Dieras, V., Lacroix-Triki, M., Lacroix, L., Cohen, P., Gentien, D., et al. (2014). Comparative genomic hybridisation array and DNA sequencing to direct treatment of metastatic breast cancer: a multicentre, prospective trial (SAFIR01/UNICANCER). Lancet Oncol. *15*, 267–274.

9. Gao, X., Li, L., Cai, X., Huang, Q., Xiao, J., and Cheng, Y. (2021). Targeting nanoparticles for diagnosis and therapy of bone tumors: Opportunities and challenges. Biomaterials *265*, 120404.

10. Sohretoglu, D., and Huang, S. (2018). Ganoderma lucidum Polysaccharides as An Anti-cancer Agent. Anticancer. Agents Med. Chem. *18*, 667–674.

11. Wang, Y., Fan, X., and Wu, X. (2020). Ganoderma lucidum polysaccharide (GLP) enhances antitumor immune response by regulating differentiation and inhibition of MDSCs via a CARD9-NF-κB-IDO pathway. Biosci. Rep. *40*, BSR20201170.

12. Wang, P.Y., Zhu, X.L., and Lin, Z.B. (2012). Antitumor and Immunomodulatory Effects of Polysaccharides from Broken-Spore of Ganoderma lucidum. Front. Pharmacol. *3*, 135.

13. Kladar, N.V., Gavarić, N.S., and Božin, B.N. (2016). Ganoderma: insights into anti-cancer effects. Eur. J. Cancer Prev. *25*, 462–471.

14. Song, Y., Fu, Y., Xie, Q., Zhu, B., Wang, J., and Zhang, B. (2020). Anti-angiogenic Agents in Combination With Immune Checkpoint Inhibitors: A Promising Strategy for Cancer Treatment. Front. Immunol. *11*, 1956.

15. Qiao, L., Liang, N., Zhang, J., Xie, J., Liu, F., Xu, D., Yu, X., and Tian, Y. (2015). Advanced research on vasculogenic mimicry in cancer. J. Cell. Mol. Med. *19*, 315–326.

16. Sun, M., Ye, Y., Xiao, L., Duan, X., Zhang, Y., and Zhang, H. (2017). Anticancer effects of ginsenoside Rg3 (Review). Int. J. Mol. Med. *39*, 507–518.

17. Hu, S., Zhu, Y., Xia, X., Xu, X., Chen, F., Miao, X., and Chen, X. (2019). Ginsenoside Rg3 Prolongs Survival of the Orthotopic Hepatocellular Carcinoma Model by Inducing Apoptosis and Inhibiting Angiogenesis. Anal. Cell. Pathol. (Amst.) *2019*, 3815786.

18. Zhang, Y., Wang, S., Dai, M., Nai, J., Zhu, L., and Sheng, H. (2020). Solubility and Bioavailability Enhancement of Oridonin: A Review. Molecules *25*, 332.

19. Ding, Y., Ding, C., Ye, N., Liu, Z., Wold, E.A., Chen, H., et al. (2016). Discovery and development of natural product oridonin-inspired anticancer agents. European journal of medicinal chemistry *122*, 102–117.

20. Xu, J., Wold, E.A., Ding, Y., Shen, Q., and Zhou, J. (2018). Therapeutic potential of oridonin and its analogs: from anticancer and antiinflammation to neuroprotection. Molecules (Basel, Switzerland) *23*, 474.

21. Liu, Z., Ouyang, L., Peng, H., and Zhang, W.Z. (2012). Oridonin: targeting programmed cell death pathways as an anti-tumour agent. Cell Prolif. *45*, 499–507.

22. Ye, Y.C., Wang, H.J., Xu, L., Liu, W.W., Liu, B.B., Tashiro, S., Onodera, S., and Ikejima, T. (2012). Oridonin induces apoptosis and autophagy in murine fibrosarcoma L929 cells partly via NO-ERK-p53 positive-feedback loop signaling pathway. Acta Pharmacol. Sin. *33*, 1055–1061.

23. Kwan, H.-Y., Yang, Z., Fong, W.-F., Hu, Y.-M., Yu, Z.-L., and Wen-Luan, H.W. (2013). The anticancer effect of oridonin is mediated by fatty acid synthase suppression in human colorectal cancer cells. J Gastroenterol *48*, 182–192.

24. Tong, X.P., Chen, Y., Zhang, S.Y., Xie, T., Tian, M., Guo, M.R., Kasimu, R., Ouyang, L., and Wang, J.H. (2015). Key autophagic targets and relevant small-molecule compounds in cancer therapy. Cell Prolif. *48*, 7–16.

25. Laffleur, F., and Keckeis, V. (2020). Advances in drug delivery systems: Work in progress still needed? Int. J. Pharm. *590*, 119912.

26. Nardin, I., and Köllner, S. (2019). Successful development of oral SEDDS: screening of excipients from the industrial point of view. Adv. Drug Deliv. Rev. *142*, 128–140.

27. Wu, C.X., Wang, X.Q., Chok, S.H., Man, K., Tsang, S.H.Y., Chan, A.C.Y., Ma, K.W., Xia, W., and Cheung, T.T. (2018). Blocking CDK1/PDK1/β-Catenin signaling by CDK1 inhibitor RO3306 increased the efficacy of sorafenib treatment by targeting cancer stem cells in a preclinical model of hepatocellular carcinoma. Theranostics *8*, 3737–3750.

28. Mazzanti, R., Gramantieri, L., and Bolondi, L. (2008). Hepatocellular carcinoma: epidemiology and clinical aspects. Mol. Aspects Med. *29*, 130–143.

29. Song, Y., Fu, Y., Xie, Q., Zhu, B., Wang, J., and Zhang, B. (2020). Anti-angiogenic agents in combination with immune checkpoint inhibitors: a promising strategy for cancer treatment. Frontiers in immunology *11*, 1956.

30. Raybould, A.L., and Sanoff, H. (2020). Combination Antiangiogenic and Immunotherapy for Advanced Hepatocellular Carcinoma: Evidence to Date. J. Hepatocell. Carcinoma *7*, 133–142.

31. Yi, M., Jiao, D., Qin, S., Chu, Q., Wu, K., and Li, A. (2019). Synergistic effect of immune checkpoint blockade and anti-angiogenesis in cancer treatment. Mol. Cancer *18*, 60.

32. Long, J., Hu, Z., Xue, H., Wang, Y., Chen, J., Tang, F., Zhou, J., Liu, L., Qiu, W., Zhang, S., et al. (2019). Vascular endothelial growth factor (VEGF) impairs the motility and immune function of human mature dendritic cells through the VEGF receptor 2-RhoA-cofilin1 pathway. Cancer Sci. *110*, 2357–2367.

33. Aggarwal, V., Tuli, H.S., Varol, A., Thakral, F., Yerer, M.B., Sak, K., Varol, M., Jain, A., Khan, M.A., and Sethi, G. (2019). Role of Reactive Oxygen Species in Cancer Progression: Molecular Mechanisms and Recent Advancements. Biomolecules *9*, 735.

34. Malo, C.S., Khadka, R.H., Ayasoufi, K., Jin, F., AbouChehade, J.E., Hansen, M.J., Iezzi, R., Pavelko, K.D., and Johnson, A.J. (2018). Immunomodulation Mediated by Anti-angiogenic Therapy Improves CD8 T Cell Immunity Against Experimental Glioma. Front. Oncol. *8*, 320.

35. Delfortrie, S., Pinte, S., Mattot, V., Samson, C., Villain, G., Caetano, B., Lauridant-Philippin, G., Baranzelli, M.C., Bonneterre, J., Trottein, F., et al. (2011). Egfl7 promotes tumor escape from immunity by repressing endothelial cell activation. Cancer Res. *71*, 7176–7186.

36. Voron, T., Colussi, O., Marcheteau, E., Pernot, S., Nizard, M., Pointet, A.L., Latreche, S., Bergaya, S., Benhamouda, N., Tanchot, C., et al. (2015). VEGF-A modulates expression of inhibitory checkpoints on CD8+ T cells in tumors. J. Exp. Med. *212*, 139–148.

37. De Sanctis, Ugel, S., Facciponte, J., and Facciabene, A. (2018). The dark side of tumor-associated endothelial cells. Semin Immunol *35*, 35–47.

38. McAllister, S.S., and Weinberg, R.A. (2014). The tumour-induced systemic environment as a critical regulator of cancer progression and metastasis. Nat. Cell Biol. *16*, 717–727.

39. Xiang, D.M., Sun, W., Zhou, T., Zhang, C., Cheng, Z., Li, S.C., Jiang, W., Wang, R., Fu, G., Cui, X., et al. (2019). Oncofetal HLF transactivates c-Jun to promote hepatocellular carcinoma development and sorafenib resistance. Gut *68*, 1858–1871.

40. Tovar, V., Cornella, H., Moeini, A., Vidal, S., Hoshida, Y., Sia, D., Peix, J., Cabellos, L., Alsinet, C., Torrecilla, S., et al. (2017). Tumour initiating cells and IGF/FGF signalling contribute to sorafenib resistance in hepatocellular carcinoma. Gut *66*, 530–540.

41. Da Ros, M., De Gregorio, V., Iorio, A.L., Giunti, L., Guidi, M., de Martino, M., Genitori, L., and Sardi, I. (2018). Glioblastoma Chemoresistance: The Double Play by Microenvironment and Blood-Brain Barrier. Int. J. Mol. Sci. *19*, 2879.

42. Xavier, C.P.R., Caires, H.R., Barbosa, M.A.G., Bergantim, R., Guimarães, J.E., and Vasconcelos, M.H. (2020). The Role of Extracellular Vesicles in the Hallmarks of Cancer and Drug Resistance. Cells *9*, 1141.

43. Gonzalez, H., Hagerling, C., and Werb, Z. (2018). Roles of the immune system in cancer: from tumor initiation to metastatic progression. Genes Dev. *32*, 1267–1284.

44. Ham, S., Lima, L.G., Lek, E., and Möller, A. (2020). The Impact of the Cancer Microenvironment on Macrophage Phenotypes. Front. Immunol. *11*, 1308.

45. Wang, Q., He, Z., Huang, M., Liu, T., Wang, Y., Xu, H., Duan, H., Ma, P., Zhang, L., Zamvil, S.S., et al. (2018). Vascular niche IL-6 induces alternative macrophage activation in glioblastoma through HIF-2α. Nat. Commun. *9*, 559.

46. Kelly, A., Gunaltay, S., McEntee, C.P., Shuttleworth, E.E., Smedley, C., Houston, S.A., Fenton, T.M., Levison, S., Mann, E.R., and Travis, M.A. (2018). Human monocytes and macrophages regulate immune tolerance via integrin αvβ8-mediated TGFβ activation. J. Exp. Med. *215*, 2725–2736.

47. Coffelt, S.B., Hughes, R., and Lewis, C.E. (2009). Tumor-associated macrophages: effectors of angiogenesis and tumor progression. Biochim. Biophys. Acta *1796*, 11–18.

48. Kuang, D.M., Zhao, Q., Peng, C., Xu, J., Zhang, J.P., Wu, C., and Zheng, L. (2009). Activated monocytes in peritumoral stroma of hepatocellular carcinoma foster immune privilege and disease progression through PD-L1. J. Exp. Med. *206*, 1327–1337.

49. De Palma, M., and Lewis, C.E. (2013). Macrophage regulation of tumor responses to anticancer therapies. Cancer Cell *23*, 277–286.

50. Sueangoen, N., Tantiwetrueangdet, A., and Panvichian, R. (2020). HCC-derived EGFR mutants are functioning, EGF-dependent, and erlotinib-resistant. Cell Biosci. *10*, 41.

51. Ito, Y., Takeda, T., Sakon, M., Tsujimoto, M., Higashiyama, S., Noda, K., Miyoshi, E., Monden, M., and Matsuura, N. (2001). Expression and clinical significance of erb-B receptor family in hepatocellular carcinoma. Br. J. Cancer *84*, 1377–1383.

52. Kang, N., Cao, S., Jiang, B., Zhang, Q., Donkor, P.O., Zhu, Y., Qiu, F., and Gao, X. (2020). Cetuximab enhances oridonin-induced apoptosis through mitochondrial pathway and endoplasmic reticulum stress in laryngeal squamous cell carcinoma cells. Toxicol. In Vitro *67*, 104885.

53. Kadioglu, O., Saeed, M., Kuete, V., Greten, H.J., and Efferth, T. (2018). Oridonin Targets Multiple Drug-Resistant Tumor Cells as Determined by *in Silico* and *in Vitro* Analyses. Front. Pharmacol. *9*, 355.

54. Pi, J., Jiang, J., Cai, H., Yang, F., Jin, H., Yang, P., Cai, J., and Chen, Z.W. (2017). GE11 peptide conjugated selenium nanoparticles for EGFR targeted oridonin delivery to achieve enhanced anticancer efficacy by inhibiting EGFR-mediated PI3K/AKT and Ras/Raf/MEK/ERK pathways. Drug Deliv. *24*, 1549–1564.

55. Tanabe, A., and Sahara, H. (2020). The Metabolic Heterogeneity and Flexibility of Cancer Stem Cells. Cancers (Basel) *12*, 2780.

56. Lee, H.Y., and Hong, I.S. (2020). Targeting Liver Cancer Stem Cells: An Alternative Therapeutic Approach for Liver Cancer. Cancers (Basel) *12*, 2746.

61. Ding, C., Zhang, Y., Chen, H., Yang, Z., Wild, C., Chu, L., Liu, H., Shen, Q., and Zhou, J. (2013). Novel nitrogen-enriched oridonin analogues with thiazole-fused A-ring: protecting group-free synthesis, enhanced anticancer profile, and improved aqueous solubility. J. Med. Chem. *56*, 5048–5058.

62. Liu, J.P., Lu, D., Nicholson, R.C., Zhao, W.J., Li, P.Y., and Wang, F. (2012). Toxicity of a novel anti-tumor agent 20(S)-ginsenoside Rg3: a 26-week intramuscular repeated administration study in rats. Food Chem. Toxicol. *50*, 3388–3396.

63. Ali, E.S., Sharker, S.M., Islam, M.T., Khan, I.N., Shaw, S., Rahman, M.A., Uddin, S.J., Shill, M.C., Rehman, S., Das, N., et al. (2021). Targeting cancer cells with nanotherapeutics and nanodiagnostics: Current status and future perspectives. Semin. Cancer Biol. *69*, 52–68.

64. Shao, B., Feng, Y., Zhang, H., Yu, F., Li, Q., Tan, C., Xu, H., Ying, J., Li, L., Yang, D., et al. (2018). The 3p14.2 tumour suppressor ADAMTS9 is inactivated by promoter CpG methylation and inhibits tumour cell growth in breast cancer. J. Cell. Mol. Med. *22*, 1257–1271.

Supplemental information

Multiple targeted self-emulsifying

compound RGO reveals obvious anti-tumor

potential in hepatocellular carcinoma

Sanxiu He, Shaorong Tian, Xiaoqian He, Xin Le, Yijiao Ning, Jialin Chen, Hongyi Chen, Junhao Mu, Ke Xu, Qin Xiang, Yue Wu, Jiong Chen, and Tingxiu Xiang
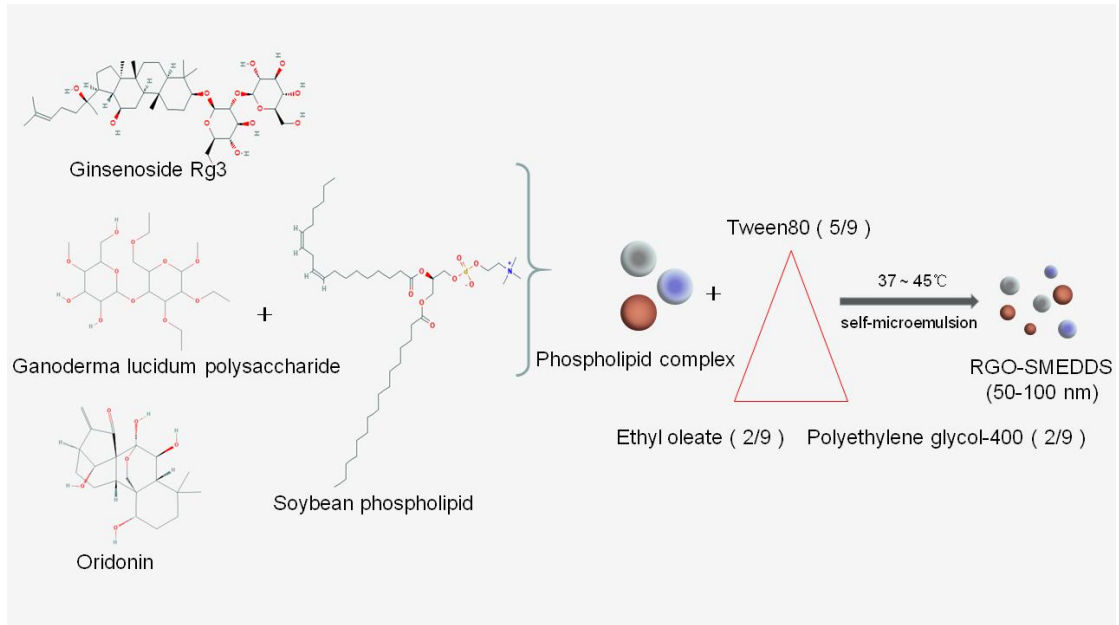
Figure S1. Schematic illustration of the preparation of RGO-SMEDDS.
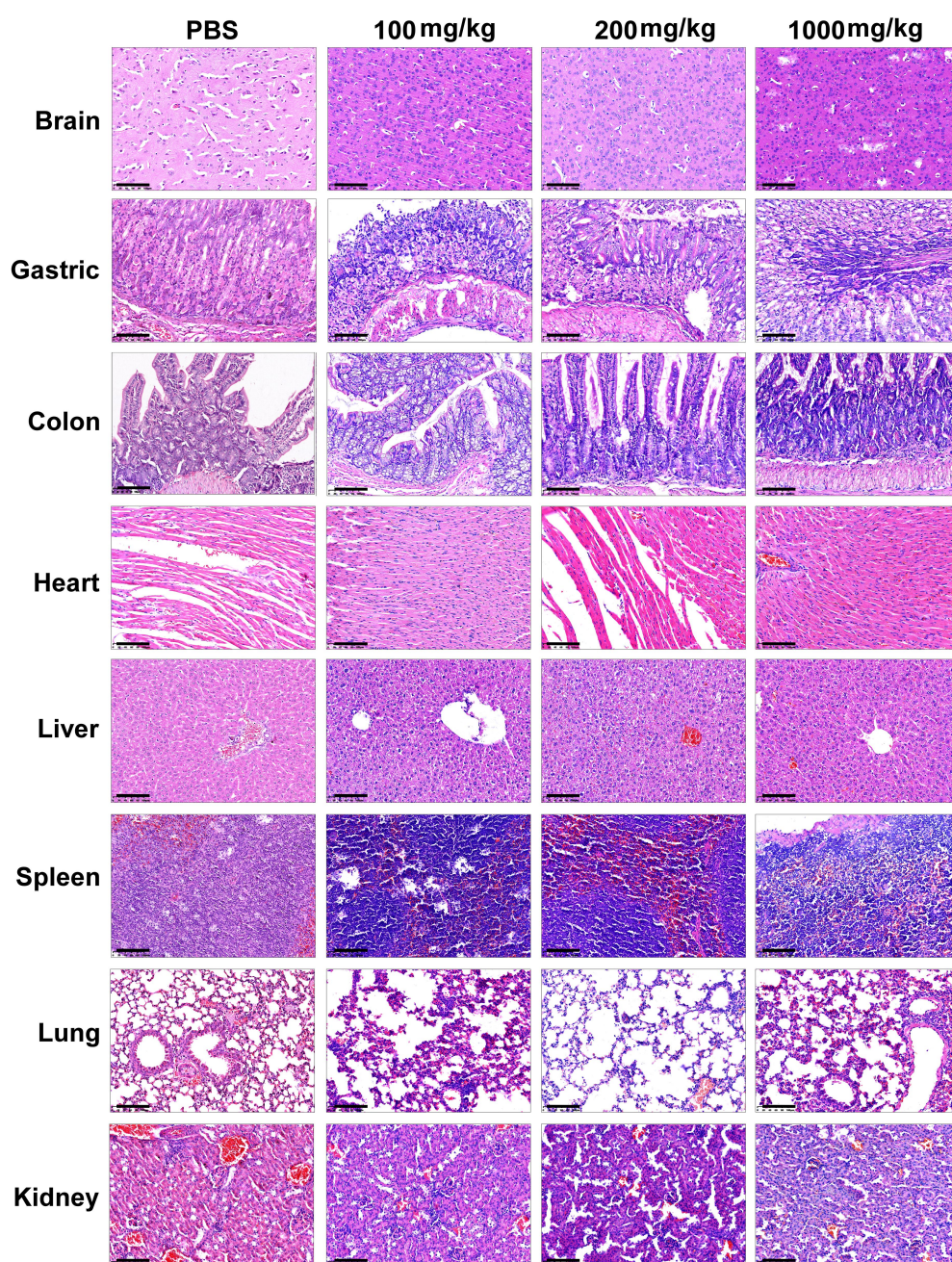
Figure S2. RGO-SMEDDS in vivo toxicity

HE staining results of major organs (brain, gastric, colon, heart, liver, spleen, lung and

kidney) showing toxicity of RGO in vivo. C57BL/6 mice after one-time oral

administration with ascending concentration order of 0, 100, 200, 1000mg/kg RGO.

Scale bar: 100 μm.